Ecological Engineering 54 (2013) 245–253

Contents lists available at SciVerse ScienceDirect

Ecological Engineering

journal homepage: www.elsevier.com/locate/ecoleng

Effectiveness of ecological restoration projects in a karst region of southwest China assessed using vegetation succession mapping

Qi Xiangkun[a,c,d], Wang Kelin[a,c,*], Zhang Chunhua[b,a,c]

[a] Key Laboratory for Agro-ecological Processes in Subtropical Region, Institute of Subtropical Agriculture, Chinese Academy of Sciences, Changsha 410125, China
[b] Department of Geography and Geology, Algoma University, Sault Ste. Marie, ON P6A 2G4, Canada
[c] Huanjiang Observation and Research Station for Karst Ecosystem, Chinese Academy of Sciences, Huanjiang 547100, China
[d] Graduate University of Chinese Academy of Sciences, Beijing 100049, China

ARTICLE INFO

Article history:
Received 17 June 2012
Received in revised form 17 January 2013
Accepted 20 January 2013
Available online 6 March 2013

Keywords:
Karst
Ecological restoration
Vegetation succession
Remote sensing
Landsat
Shadow effects
Topographic correction

ABSTRACT

From the 1950s to 1980s, the rapid disappearance of vegetation led to severe environmental degradation in the karst region of southwest China. Projects to restore vegetation have been applied in this area since the 1990s. However, few studies have evaluated the effects of restoration on karst vegetation. Vegetation succession, an ecological phenomenon involving predictable changes in plant communities, can serve as an indicator of environmental changes. Remote-sensing techniques have been utilized to map vegetation communities and succession at regional scales. However, shadows caused by the rough karst landforms in this area of China make the application of remotely sensed imagery challenging. Here, we used three Landsat Thematic Mapper images from 1990, 2004, and 2011 to examine whether various image pre-processing methods (vegetation indices, topographic correction, and minimum noise fraction [MNF] transformation) and a digital elevation model improved image classification. Using a maximum likelihood classifier, vegetation communities were classified into five classes (successional stages) of grass, grass–shrub, shrub, tree–shrub, and forest. The results indicated that a combination of inverse MNF transformed bands, the normalized difference moisture index (NDMI), and the moisture stress index (MSI) minimized topographic effects and consequently produced the best input for imagery classification and provided the best classification results and showed ongoing vegetation succession in the study area from 1990 to 2011. Dominant vegetation communities had shifted from early successional stages (i.e., grass and grass–shrub) in 1990 to forest and tree–shrub in 2011. Increases in patch number and average patch area for forest and tree–shrub communities at the class level suggested the expansion of these two communities. Enhanced patch connectivity and aggregation at the landscape level indirectly signified decreases in disturbances to forest and tree–shrub communities. These results demonstrate that ecological restoration and reconstruction efforts in the area have helped to restore vegetation cover.

1. Introduction

Vegetation is a critical environmental component for food production, resource conservation (Woo et al., 1997), nutrient cycling, and carbon sequestration (Goodale et al., 2002; Kuplich, 2006). Vegetation succession, which is an ecological phenomenon involving predictable changes in plant communities, can serve as an indicator of environmental changes (Pregitzer and Euskirchen, 2004). Although succession has been well documented in a variety of landscapes (Foody et al., 1996; Helmer et al., 2000; Song and Woodcock, 2002; Liu et al., 2008), few studies have examined karst environments, a unique landscape formed above carbonate bedrock. Southwest China has one of the largest continuous karst landscapes in the world, spanning an area about 540,000 km^2 (Su, 2002). Karst is among the most fragile environments worldwide (Legrand, 1973; Parise and Gunn, 2007). Inappropriate agricultural practices and over-exploitation on sloping lands were common in the last half of the twentieth century and contributed to the rapid decrease in karst forests in southwest China (Stokes et al., 2010; Wen et al., 2011). Beginning in the 1990s, several ecological projects, such as the Green for Grain program and mountain closures (providing living allowances and banning logging), were implemented to restore vegetation cover in this area. Remote-sensing techniques, which have long been applied to examine vegetation communities (Foody et al., 1996; Song et al., 2007), can be used to monitor changes in plant communities and assess

* Corresponding author at: Key Laboratory for Agro-ecological Processes in Subtropical Region, Institute of Subtropical Agriculture, Chinese Academy of Sciences, Changsha 410125, China. Tel.: +86 731 84615201; fax: +86 731 84612685.
E-mail address: kelin@isa.ac.cn (K. Wang).

0925-8574/$ – see front matter © 2013 Elsevier B.V. All rights reserved.
http://dx.doi.org/10.1016/j.ecoleng.2013.01.002

the effects of ecological restoration projects on vegetation conditions.

The general natural successional stages in this karst region are grass, grass–shrub, shrub, tree–shrub, and forest (Li et al., 2004; Peng et al., 2012). Grass is an early successional stage, and its average height is generally not more than 0.9 m (Yu et al., 2000; Wen et al., 2011). Dominant species within the karst grass communities are *Microstegium vagans*, *Pteridium aquilinum*, and *Imperata cylindrical*. Grass–shrub is the transitional successional stage from grass to shrub, with an average height ranging from 0.9 to 1.2 m. Dominant grass–shrub species include *Saccharum arundinaceum* and *Vitex negundo*. Plants in the shrub stage range in height from 1.2 to 2 m, with dominant species including *Rhus chinensis*, *Pyracantha fortuneana*, *Rosa laevigata*, and *Cipadessa cinerascens*. The shift from a grass to shrub community generally takes 10–15 years in the absence of severe disturbances. Tree–shrub is the transitional community from shrub to forest, and the height of this community is about 2–4 m. Dominant species include *Alchornea trewioides*, *Sapium rotundifolium*, *Gleditsia fera*, and *Broussonetia kazinoki*. Mature forests harbor dominant species of *Cyclobalanopsis glauca*, *Choerospondias axillaris*, and *Sterculia nobilis*. Without severe human disturbance, the ongoing succession from a grass community to a forest generally takes 30–50 years in this karst region (He et al., 2008). Although reforestation has been implemented along with restoration (common introduced non-native tree species are *Pinus massoniana* and *Radermachera sinica*), the targeted area is limited (1–2% of the study area). Natural succession is dominant because of geological background limitations.

Research on karst vegetation succession has generally relied on field surveys (e.g., Yu et al., 2000; Li et al., 2004; Tang et al., 2010), which are time consuming, expensive, and limited in spatial coverage (Song et al., 2007). Hence, comprehensive understanding of vegetation succession in the karst environment is lacking at a regional scale. Each vegetation successional stage (community) exhibits different tree species composition, canopy structure, and stand height, and consequently has a unique spectral response in satellite images (Song and Woodcock, 2002; Verbesselt et al., 2010). Landsat imagery is useful for mapping vegetation communities because it can provide medium spatial resolution and a four-decade historical archive of the Earth's land surface (Schroeder et al., 2007; Liu et al., 2008; Lee and Yeh, 2009; Mello and Alves, 2011). Vegetation succession can therefore be mapped by detecting changes (Foody et al., 1996; Lucas et al., 2002).

Variations in solar illumination and terrain conditions in mountainous regions can affect the extraction of vegetation information from satellite imagery (Gao and Zhang, 2009). Topography can cause bidirectional reflectance and shadow effects, consequently altering surface reflectance (Song and Woodcock, 2003). In China, hills and mountains cover two-thirds of the land surface. Many ecological restoration and reconstruction projects (e.g., the Natural Forest Protection Project [NFPP], the Green for Grain program, and some regional ecological projects such as the Loess Plateau treatment project) have aimed to restore vegetation cover on degraded lands, especially steeply sloped land (Yu et al., 2011). The rough karst landscape in southwestern China, which has formed by alternating stages of uplift and relative stability in Cenozoic carbonate rock (Wang et al., 2004a), produces substantial shadowing in Landsat images. Weak reflectance from such shaded areas complicates the classification of vegetation communities. These topographical effects are a limiting factor when using remote sensing to monitor vegetation succession in karst regions. However, few researchers have attempted to minimize topographic effects when extracting vegetation community information in karst regions. For effective use of remotely sensed imagery in the evaluation of ecological restoration projects, mitigation of topographic effects is important.

Various image pre-processing methods have been applied to minimize the effects of shadows on image classification. These methods include band ratios (e.g., Lyon et al., 1998; Helmer et al., 2000; Huang and Cai, 2009), additional topographic data (e.g., Senoo et al., 1990; Liu et al., 2002), and topographic correction (e.g., Tokola et al., 2001; Riano et al., 2003; Cuo et al., 2010). Band ratios can minimize changes in solar illumination caused by variations in slope and aspect (Elvidge and Lyon, 1985). Helmer et al. (2000) reported that topography had less of an effect on the Landsat band 4/5 ratio in a mountainous tropical forest. Song and Woodcock (2003) demonstrated that simulated NDVI is resistant to topographic effects at all illumination angles. The normalized difference moisture index (NDMI) and tasseled cap wetness have also been used to classify forest types (Wilson and Sader, 2002; Jin and Sader, 2005). The use of digital elevation models (DEM) in vegetation classification in mountainous regions has also proven useful in improving the classification accuracy, if the distribution of vegetation is determined by altitude (Franklin et al., 2002). Topographic correction models have also been applied to Landsat images has been shown to increase classification accuracies (Tokola et al., 2001; Gao and Zhang, 2009). In addition, minimum noise fraction (MNF) transformation has been used to extract high-quality end members (Green et al., 1988) for image classification. However, few studies have explored the potential of this method to reduce noise from shadow effects.

This study aimed to assess the effects of ecological restoration and reconstruction projects on vegetation recovery in a karst region in southwest China by vegetation succession mapping. Various band combinations were classified using a maximum likelihood classifier to extract vegetation community information. Pattern characteristic analyses were also applied to examine changes in karst vegetation communities.

2. Materials and methods

2.1. Study area

The study area (107.55°E, 25.00°N) was a karst region in Huanjiang County, Guangxi Province, southwest China. The region is hilly with an area of 56,300 ha. Elevation ranges from 230 to 1031 m (Fig. 1). The climate is warm–moist subtropical, with a mean annual precipitation of 1389 mm and a mean annual temperature of 19.9 °C. Typical landforms in this region are tower karsts and depressions, with 66% of the study area having slope angles steeper than 25°. Although the climatic vegetation community climax in this area is subtropical evergreen forest, a variety of successional stages (vegetation communities) exist because of severe human disturbances and geological background limitations. This area has a relatively high population density (52 people per km^2) and a history of more than 1000 years of agricultural development. Tree cutting for timber and charcoal and active agricultural practices on the slopes led to the disappearance of the climax community from the 1950s through the 1980s in this region. By the 1990s, 60–70% of the forested area in the karst regions was cleared, and most existing forests were secondary vegetation (Wen et al., 2011). Contiguous forest (subtropical evergreen forest communities) could only be found in the north of the study region, where the Mulun National Reserve was established to protect karst species diversity. In contrast, vegetation communities outside the reserve experienced serve human disturbances (e.g., logging, grazing, and excessive cultivation). Therefore, the continuous subtropical evergreen forest communities (forest stage) hardly had been found in 1990 and most existent vegetation communities outside the reserve are grasses or shrubs. In these areas, karst rocky desertification occurred with

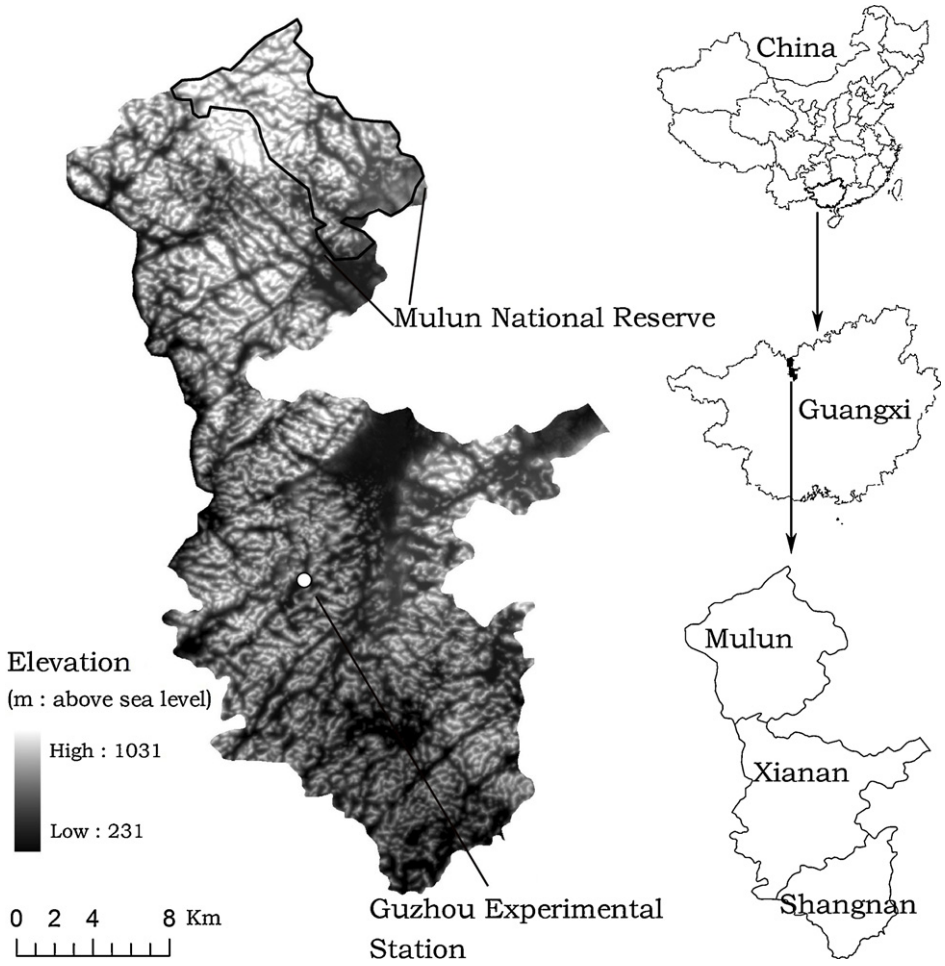

Fig. 1. Terrain of the Huanjiang karst region in Southwest China. The study area included three towns: Mulun, Xianan, and Shangnan.

widespread exposed bedrock, declining land productivity, and the formation of desert-like landscapes (Zhang et al., 2011). To restore the degraded karst environment, the Guzhou Experimental Station, whose task is ecological restoration and reconstruction in fragile karst regions, was established in this region.

2.2. Satellite image processing

Three Landsat-5 Thematic Mapper (TM) images taken on 18 May 1990, 8 May 2004, and 28 May 2011 were downloaded from the Center for Earth Observation and Digital Earth, China (http://www.ceode.cas.cn/sjyhfw/). Close imagery acquisition dates facilitate the minimization of noise effects caused by differences in sun elevation angle and phenology (Song and Woodcock, 2003). A 1:50,000 scale DEM was obtained for topographic correction and classification.

All satellite images were subjected to data pre-processing procedures including atmospheric calibration and geo-referencing. The DOS3 algorithm (Song et al., 2001) was applied to each image to remove irradiation differences caused by the atmosphere. Each image was then geometrically corrected with 18–25 ground control points (GCPs). The GCPs were collected using two MobileMapper GPS units (Thales Navigation Inc., USA), one acting as the base station and another as the rover. The positional accuracy of these GCPs was within 1 m. The root mean-square (RMS) errors for all geometric corrections were less than 0.5 pixels. These three images were resampled to a 30-m resolution using the nearest-neighbor resampling method and then projected to a Universal Transverse Mercator (UTM) projection.

2.3. Topographic correction

Vegetation indices (NDVI (1), NDMI (2)) and the moisture stress index (MSI) (3) were computed as optional classification input. A shadow index (SI) (4) (Roy et al., 1996) was used to represent the shadow caused by topographic effects. These indices were computed as follows:

$$\mathrm{NDVI} = \frac{\mathrm{TM4} - \mathrm{TM3}}{\mathrm{TM4} + \mathrm{TM3}} \quad (1)$$

$$\mathrm{NDMI} = \frac{\mathrm{TM4} - \mathrm{TM5}}{\mathrm{TM4} + \mathrm{TM5}} \quad (2)$$

$$\mathrm{MSI} = \frac{\mathrm{TM5}}{\mathrm{TM4}} \quad (3)$$

$$\mathrm{SI} = \sqrt[3]{(256 - \mathrm{TM1})(256 - \mathrm{TM2})(256 - \mathrm{TM3})} \quad (4)$$

where TM1, TM2, TM3, TM4, and TM5 are Landsat TM blue, green, red, near infrared, and middle infrared bands.

MNF transformation was applied to minimize topographic impacts. The second forward MNF transformed band was very strongly correlated with SI, indicating that this band was dominated by shadow information. Consequently, the band was excluded from the inverse MNF transformation.

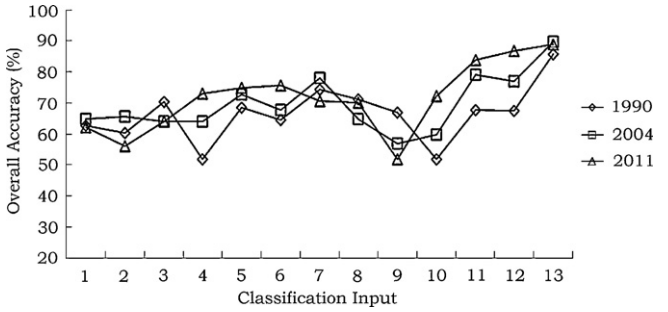

Fig. 2. Overall accuracy of various classification inputs for 1990, 2004, and 2011 imagery. Note: 1, six TM bands; 2, six TM bands and DEM; 3, six TM bands (C-corrected); 4, six TM bands and NDVI; 5, six TM bands and NDMI; 6, six TM bands and MSI; 7, six TM bands, NDMI, and MSI; 8, NDMI and MSI; 9, six inverse MNF bands; 10, six inverse MNF bands and NDVI; 11, six inverse MNF bands and NDMI; 12, six inverse MNF bands and MSI; 13, six inverse MNF bands, NDMI, and MSI.

Topographic correction was also applied to the satellite images to reduce the spectral variation in ground objects caused by terrain relief (Riano et al., 2003). According to the minimum principle of correlation coefficients between image radiance values and the cosine values of solar incidence angles (Gao and Zhang, 2009), the C correction (Teillet et al., 1982) was selected to correct the satellite images:

$$R_H = R_T \left(\frac{\cos\theta_p + C_\lambda}{\cos\gamma_i + C_\lambda} \right) \quad (5)$$

where R_H is the corrected radiance of the image, R_T is the uncorrected radiance of the image, θ_p is the slope angle, γ_i is the incident solar angle on a horizontal surface, and C_λ is a coefficient calculated from the regression line between R_T and the cosine of the incident solar angle ($\cos\gamma_i$). $\cos\gamma_i$, the illumination, is calculated as (Smith et al., 1980):

$$\cos\gamma_i = \cos z \cos\theta_p + \sin z \sin\theta_p \cos(e - \theta_a) \quad (6)$$

where z and e are solar zenith angle and azimuth, respectively, and θ_p and θ_a are the slope and aspect of the terrain, respectively.

2.4. Vegetation successional stage classification

Various combinations of vegetation indices, MNF bands, and Landsat TM bands were used as classification inputs. Each combination was classified into five successional classes: grass, grass–shrub, shrub, tree–shrub, and forest. Built-up areas are limited in this region because of local biophysical conditions. Therefore, the built-up land area was merged with cropland as one class in the classification. Training areas were selected through visual interpretation and field observations. Information from interviews with local residents and historical land cover maps were also used in training area selection.

A widely used maximum likelihood classifier was applied for the classification of 1990, 2004, and 2011 images. Accuracy assessments were conducted using error matrices. Reference points for accuracy assessments were generated using a stratified random method. Class labels (vegetation community types) of these points were determined by visual interpretation of Landsat imagery, IKONOS imagery from 23 May 2004, field collected data from 2007 to 2011, and historical vegetation condition information collected from interviews with local people. Totals of 260, 264, and 279 reference points were collected to assess the classification accuracy of the 1990, 2004, and 2011 images, respectively. Different classification accuracies were achieved from various inputs (Fig. 2). Image pre-processing and classification were completed using ERDAS IMAGINE 8.5 (LLC Inc., USA) and ArcGIS 9.2 (ESRI Inc., USA).

A transform matrix was applied to quantitatively describe changes in vegetation communities. The net change ratio (NCR) (7) is often used (Dong et al., 2009) to indicate the change in each successional stage from a starting year to an end year. The rate (Ti) (8) represents the dynamics of successional stages from the starting year to the end year. K (9) is the NCR of each year. They are defined as follows:

$$\mathrm{NCR} = \frac{A_{ie} - A_{is}}{A_{is}} \times 100\% \quad (7)$$

$$\mathrm{Ti} = \sum_{j=1}^{n-1} \frac{T_{ij}}{L_{t_0}} \times 100\% \quad (8)$$

$$K = \frac{A_{ie} - A_{is}}{A_{is}} \times \frac{1}{T} \times 100\% \quad (9)$$

where A_{is} is the area of the ith vegetation successional stage in the starting year, and A_{ie} is the area of the ith vegetation successional stage in the end year. Ti is the ratio of the change in the ith vegetation successional stage from the start date t_0 to the end date t_k. T_{ij} is the area transforming from the ith successional stage to the jth successional stage. L_{t_0} is the area of the ith successional stage at date t_0. T is the number of years between two dates of image acquisition.

2.5. Landscape pattern analysis

To determine the conditions of karst vegetation succession, landscape pattern analysis was further applied to the vegetation community maps on various dates at the class and landscape levels using FRAGSTATS 3.3. Six metrics at the class level were selected to represent the patch area, shape, fragmentation, and spatial structure of each successional stage. These metrics were the patch number (NP), average patch area (AREA_MN), radius of gyrate (GYRATE_MN), area-weighted shape index (AWMSI), aggregation index (AI), and lumpiness (CLUMPY). Seven metrics at the landscape level were used to represent changes in vegetation succession at a landscape scale: NP, AREA_MN, the contagion index (CONTAG), the interspersion and juxtaposition index (IJI), Shannon's diversity index (SHDI), Shannon's evenness index (SHEI), and AI.

3. Results and discussion

3.1. Classification of karst vegetation communities

The use of the DEM and/or topographic correction did not improve the classification of vegetation successional stages. When compared to overall accuracies from the combination of six TM bands (63%, 65%, and 62% in 1990, 2004, and 2011 respectively), overall accuracies from the combination of the six TM bands and DEM (Fig. 2, classification input 2) changed by only −2%, 1%, and −6%, respectively. Most tower karsts in this region are between 50 and 250 m high, and the climatic environment and geologic background are consistent from the bottom to the top of towers. Consequently, the distribution of vegetation communities in the study area is not determined by altitude. Therefore, it is not necessary to incorporate a DEM when classifying the vegetation communities. Similarly, topographic correction contributed little to the vegetation classification, with overall accuracies only increasing from 1% to 7% for the three images (Fig. 2, classification input 3). Topographic correction is effective for reducing the effects of terrain on spectral reflectance, and it consequently increases classification accuracy when slope angles are less than 30° (Song and Woodcock, 2003). However, 46% of the study area has slope

angles greater than 40°, thus limiting the efficiency of the topographic correction model.

The inverse MNF transformed imagery, which excluded information from the second forward MNF band, was less affected by topography. Strong correlations between the second forward MNF band and SI ($r = 0.77$, $P < 0.01$) indicated the existence of topographic information in this MNF band. Correlations between the inverse MNF transformed bands and SI were lower than those between the bands of TM imagery and SI. For example, the correlations between band 4 and band 5 of the 2011 TM imagery and SI were −0.76 and −0.77 ($P < 0.01$), respectively. In contrast, correlations with band 4 and band 5 of the 2011 inverse MNF imagery were only −0.27 and −0.48, respectively. These results indicate weaker topographic effects in the inverse MNF bands. However, classification accuracies using the inverse MNF transformed imagery (Fig. 2, classification input 9) were lower than those using TM bands in 2004 and 2011 (57% vs. 65% in 2004 and 52% vs. 62% in 2011), mainly due to the loss of vegetation information because of the exclusion of the second forward MNF band.

NDMI and MSI were better than NDVI for karst vegetation classification (Fig. 2, classification inputs 5–8, VS classification input 4). The former two indices are theoretically similar to wetness from the tasseled cap transformation (Crist and Cicone, 1984; Wilson and Sader, 2002). Wetness has proven useful for forest change detection (Collins and Woodcock, 1996; Franklin et al., 2000). In karst regions, vegetation at different successional stages exhibits obvious differences in water content, especially in the dry season, because of restrictions by the geological background. The roots of vegetation in later successional stages can grow farther into rock cracks and can consequently acquire deeper karst water than can vegetation in earlier successional stages (Nie et al., 2012). The addition of NDMI and MSI improved the classification accuracies of vegetation successional stages; accuracies increased from 2% to 26% for the three dates (Fig. 2, classification inputs 5–8, 11–13). In fact, classification using inverse MNF transformed bands, NDMI, and MSI had the highest overall accuracy (86%, 90%, and 89% in 1990, 2004, and 2011, respectively). When compared with results using the TM bands (Fig. 2, classification input 1), overall accuracies increased by 23%, 25%, and 26% in 1990, 2004, and 2011, respectively. The loss of vegetation information in the inverse MNF transformed bands may be supplemented by NDMI and MSI.

3.2. Changes in vegetation communities

The vegetation communities in the study area showed recovery from 1990 to 2004 (Fig. 3a). Shrub and grass–shrub communities were dominant in 1990, accounting for 27.2% and 18.7% of the study area, respectively. In 2004, their areas had decreased by 23.8% and 8.0%, respectively. A substantial portion (34.6%, 5289.8 ha) of shrub transformed to tree–shrub, and 39.0% (4095.1 ha) of grass–shrub and 27.5% (1801.4 ha) of grass changed to shrub. In addition, 13.7% (896.9 ha) of grass evolved to grass–shrub, and 38.7% (4281.1 ha) of tree–shrub and 12.3% (1883.2 ha) of shrub evolved to forest. Consequently, the area of forest increased by 45.9% (4452.4 ha) from 1990 to 2004 (Table 1), with a mean annual expansion rate of 3.1%. The forested area only accounted for 17.2% of the study area in 1990, most of which was in the national reserve. In contrast, the percentage of forested land had increased to 25.1% by 2004. Accordingly, grass–shrub shrank substantially (−6006.6 ha), with a mean annual decrease rate of 3.8%. In addition, 30.8% (988.9 ha) of cropland was converted to grassland.

Most vegetation communities, especially grass and grass–shrub, further developed to higher successional stages from 2004 to 2011 (Fig. 3b). For example, 72.6% (4666.7 ha) of grass evolved to grass–shrub and shrub, and 71.2% (3043.1 ha) of grass–shrub was

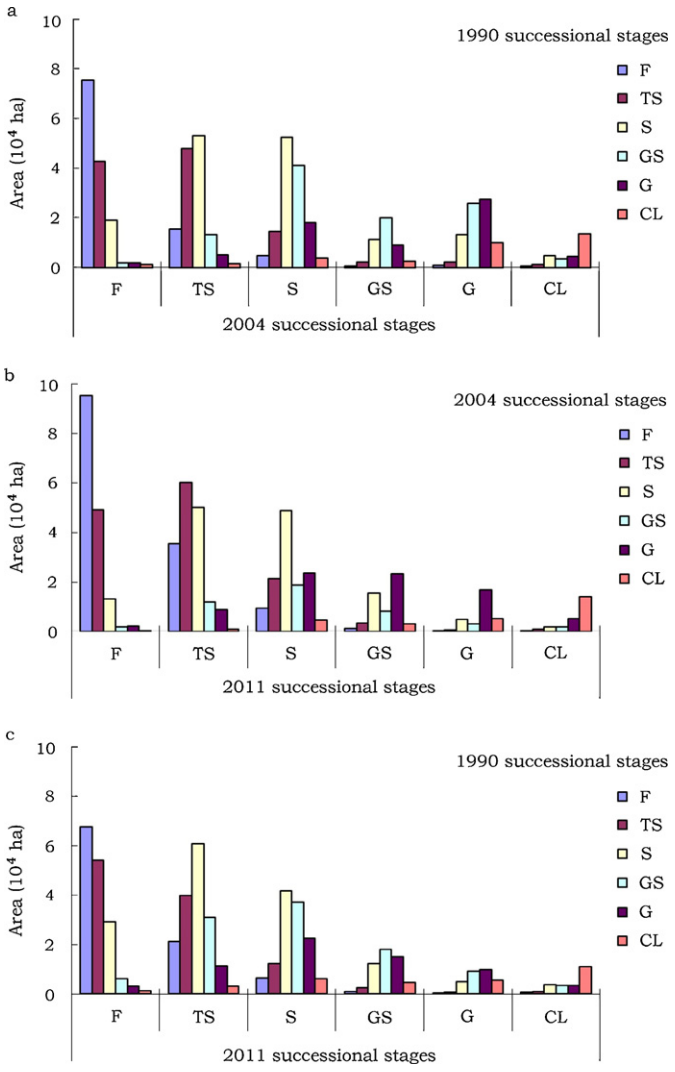

Fig. 3. Changes in vegetation communities in the Huanjiang karst region from 1990 to 2011 (Unit: ha). The labels a, b, and c are transformations of vegetation communities from 1990 to 2004, from 2004 to 2011, and from 1990 to 2011, respectively. The area of the class indicated along the *x*-axis is that of the vegetation successional stage in the later year. The area with a different color indicates the vegetation successional stage in the former year. Note: F, forest; TS, tree–shrub; S, shrub; GS, grass–shrub; G, grass; CL, cropland.

replaced by shrub and tree–shrub. Meanwhile, 37.5% (5013.5 ha) of shrub evolved to tree–shrub, and 44.7% (4915.6 ha) of tree–shrub transformed into forest. By 2011, forests accounted for 28.7% of the study area. During this time period, areas of tree–shrub also significantly expanded (3174.7 ha), with a mean annual growth rate of 3.3% (Table 1). Most of these tree–shrub communities evolved from shrub. In contrast, a further reduction in cropland area occurred, with 18.4% (507.8 ha) and 16.0% (442.6 ha) of cropland being converted to grassland and shrub, respectively. Although some croplands had transformed to grassland, the area of grassland decreased significantly, with a mean annual rate of decrease of 8.8%.

Similarly, vegetation of early successional stages progressed to later successional stages from 1990 to 2011 (Table 1 and Fig. 3c). The percentages of forest and tree–shrub increased by 66.7% (6472.4 ha) and 51.4% (5678.6 ha), respectively. In contrast, the spatial extent of shrub, grass–shrub, and grass decreased by 17.4% (2657.5 ha), 48.9% (5137.5 ha), and 53.5% (3495.5 ha), respectively. Grass and grass–shrub together accounted for 30.3% of the total

Table 1
Changes in successional stages in the Huanjiang karst region. NA is the net area of changes in different vegetation successional stages from the former year to the later year. Ti represents the dynamics of each successional stage from the former year to the later year. NCR is the ratio of net area change from the former year to the later year. *K* is the annual NCR.

Stage	1990–2004				2004–2011				1990–2011			
	NA (ha)	Ti (%)	NCR (%)	*K* (%)	NA (ha)	Ti (%)	NCR (%)	*K* (%)	NA (ha)	Ti (%)	NCR (%)	*K* (%)
F	4452.4	22.3	45.9	3.1	2020	32.6	14.3	2	6472.4	30.5	66.7	3.2
TS	2504	56.8	22.7	1.5	3174.7	55.5	23.4	3.3	5678.6	64	51.4	2.4
S	−1880.6	65.8	−12.3	−0.8	−777	63.6	−5.8	−0.8	−2657.5	72.7	−17.4	−0.8
GS	−6006.6	81	−57.2	−3.8	869.1	81.8	19.3	2.8	−5137.5	82.7	−48.9	−2.3
G	1374.4	58.2	21	1.4	−4869.9	78.9	−61.5	−8.8	−3495.5	85	−53.5	−2.5
CL	−443.6	57.8	−13.8	−0.9	−416.9	49.3	−15.1	−2.2	−860.5	65.4	−26.8	−1.3

area in 1990. By 2011, the percentages of these two communities had decreased to 9.6%. Meanwhile, the proportion of forest and tree–shrub together increased from 36.9% in 1990 to 58.4% of total area in 2011.

3.3. Changes in the vegetation landscape pattern

The pattern characteristics of vegetation succession, which highlight changes in the area and structure of vegetation communities, signify the recovery of karst vegetation in the study area from 1990 to 2011, both at the community and landscape levels. Increases in AREA_MN of forest and tree–shrub patches confirmed the expansion and aggregation of these two communities (Table 2). GYRATE_MNs of forest and tree–shrub patches had increased by 2011, which indicated better connectivity inside patches in forest and tree–shrub communities. This result may be attributed to reduce disturbances in these two communities. In contrast, the decrease in GYRATE_MNs for shrub and grass–shrub patches indicated that patches of these two communities became smaller and less well connected. Grass had the lowest shape index (AWMSI), signifying a simple shape, and human disturbances were reduced (Yang et al., 2011). Increases in AI and CLUMPY for each successional stage (excluding grass–shrub) patch indicated that the areas of vegetation communities increased from 1990 to 2011. The NP of cropland patches decreased and the AREA_MN increased from 1990 to 2011 (Table 2), indicating the centralization of cropland distribution. These results were consistent with those from GYRATE_MN, AI, and CLUMPY of the cropland patches.

Karst vegetation communities in the study area had become more aggregated at the landscape level (Table 3) by 2011. NP decreased and CONTAG increased at the landscape level, suggesting that vegetation communities were less fragmented in 2011 than in 1990. The decrease in landscape IJI indicated a reduced degree of mixtures of vegetation communities, which also showed the expansion of several dominant vegetation communities. Furthermore, declines in SHDI and SHEI indicated that the landscape was dominated by fewer vegetation communities (i.e., forest and tree–shrub). In addition, the increase in landscape AI implied that disturbances to vegetation at the landscape level had declined and the connectivity of vegetation successional stages had increased.

3.4. Effects of ecological restoration projects on vegetation succession

Changes in vegetation communities during the 21-year study period could be explained by the implementation of a series of ecological projects. These restoration projects, including mountain closures, the Green for Grain program, and agricultural restructuring, were initiated in the 1990s. The mountain closure measure was enforced to recover vegetation cover and consequently control rocky desertification (Zhang et al., 2011). Vegetation recovery is slow in karst regions because of restrictive features of the geological environment, such as shallow soil and geological water shortages (Wang et al., 2004b; Zhang et al., 2011). Consequently, stringent measures are necessary for vegetation restoration. Therefore, the mountain closure measures have prohibited logging, industrial, and agricultural activities in the degraded region. Since the late 1990s, mountain closure measures have been applied to one-third of the study area by the county Forest Service. Individuals caught harvesting timber from natural forests are fined. Farmers have also been made more aware of environmental protection through flyers and presentations describing the mountain closure policy. In addition, the local government has subsidized local farmers to build biogas (methane) generation pits. Meanwhile, access to electricity has increased in rural areas (Table 4). The use of biogas and electricity for cooking and heating has substantially decreased the demand for fuel wood, therefore minimizing the disturbance to vegetation. Our results indicated that about half (51.8%) of vegetation communities in the study experienced recovery from 1990 to 2011. The implementation of mountain closure measures likely played a crucial role in this process.

The Green for Grain program has been managed by Forest Services at different levels in karst regions, Southwest China since 2001. This program aims to change cropland on steep slopes to forests by giving farmers grain and financial subsidies. Farmers in the study area could receive 2250 kg of grain and 300 Yuan (1 US$ equals approximately 6.3 Yuan) every year for every restored hectare of forest and pasture (Yu et al., 2011). Most farmers abandoned steeply sloped farmland to allow vegetation restoration after they received the subsidy. As part of the Green for Grain program, reforestation also carried out on the abandoned cropland to promote the implementation of the program. Although sloping croplands accounted for only 5.7% of the study area in 1990, these areas were considered one of the most important contributors to karst environmental deterioration (Wang et al., 2004b). The most severe human disturbances generally occurred on sloping cropland (Chen et al., 2012). Cultivation methods on sloping karst land often involved slash-and-burn techniques to prevent weed and shrub invasion, causing a series of ecological degradations. Therefore, monitoring of changes in sloping cropland is a very important task for ecological restoration. Our results indicated that implementation of the Green for Grain program was responsible for the conversion of 26.8% (860.5 ha) of cropland to forested land during the study period.

Provincial governments also subsidized migration in the late 1990s to compliment vegetation restoration projects (Green Committee Offices, 2001). This migration policy encouraged farmers living in the karst region to move to non-karst areas having sufficient cropland for cultivation. The population of the study area decreased from 32,990 in 1990 to 30,590 in 2011. This drop in population density in the karst region resulted in decreased human pressures on the environment, facilitating the recovery of vegetation and slowing the progress of deforestation. Our results indicate that vegetation recovery in the middle of the study area

Table 2
Landscape metrics of vegetation succession at the class level in the Huanjiang karst region.

Stage	NP		AREA_MN (ha)		GYRATE_MN (m)		AWMSI (ha)		AI (%)		CLUMPY	
	1990	2011	1990	2011	1990	2011	1990	2011	1990	2011	1990	2011
F	4786	4638	2.03	3.59	42.80	44.95	7.01	8.65	72.68	79.78	0.67	0.71
TS	10,966	7808	1.01	2.11	36.76	45.03	3.57	7.10	54.93	66.32	0.44	0.52
S	8419	9993	1.82	1.27	47.42	38.59	6.70	4.39	57.12	60.40	0.41	0.49
GS	9180	8151	1.14	0.63	39.35	31.07	4.39	2.28	54.91	49.97	0.45	0.45
G	9346	4147	0.70	0.72	32.23	32.61	3.04	2.16	48.40	55.70	0.42	0.53
CL	3489	1327	0.92	1.81	31.51	38.46	2.79	4.34	65.92	76.61	0.64	0.76

Table 3
Landscape metrics of vegetation succession at the landscape level in the Huanjiang karst region.

Year	NP	AREA_MN (ha)	CONTAG (%)	IJI (%)	SHDI	SHEI	AI (%)
1990	46,186	1.22	21.54	75.60	1.70	0.95	58.45
2011	36,064	1.56	29.69	72.56	1.56	0.87	67.35

Table 4
Population and economic statistics for the study area. ML: Mulun; XN: Xianan; SN: Shangnan. GDP represents gross domestic production. Yuan is the Chinese currency unit, with 1 US$ equal to approximately 6.3 Yuan.

Year	Total population			Percentage of farmers having access to electricity (%)			Annual per capita GDP (Yuan)	Percentage of agricultural income in GDP (%)
	ML	XN	SN	ML	XN	SN		
1990	5690	20,677	6619	28	57.9	42.8	657	42.2
2004	5628	19,866	5865	74.9	96.6	75.2	3383	41.4
2011	5944	19,000	5642	96	100	98.6	11,665	39.1

(Xianan) was farther along than in Mulun and Shangnan: 60.2% of vegetation communities in Xianan had experienced recovery, compared to 53.6% and 46.9% in the Shangnan and Mulun regions, respectively. Population reduction may be one main cause of regional differences in vegetation recovery (Table 4): the higher the population reduction, the better the vegetation recovery. Populations in the Xianan and Shangnan regions decreased by 1677 and 977, respectively, while the population in Mulun increased by just 254 from 1990 to 2011 (Table 4). These changes are primarily because many farmers from Xianan relocated to non-karst areas. In addition, urbanization affected vegetation restoration in this region. Data from household questionnaire surveys indicated that since 2000, 20% to 30% of agricultural labor forces in the study area had worked in cities during the off-season for farming, further reducing dependence on farming and forestry. Consequently, many sloping croplands were abandoned (Chen et al., 2012) and gradually became covered by grass and/or shrub over several years.

3.5. Vegetation succession in the study area

In total, 51.8% of vegetation communities in the study area had experienced ongoing succession. For example, the subtropical evergreen forest communities (forest stage) in 1990 only had been distributed continuously in the national reserve rather than outside of the reserve. After the implementation of restoration projects, the contiguous forest communities have presented to outside the reserve, especially the middle of the study area (Fig. 4). The stable structure of later successional stage communities is critical for preventing soil erosion and protecting the fragile karst ecosystem (Genet et al., 2010). However, 14.7% of vegetation communities in the study area had degraded. Although the population density in the karst region decreased, many people remained and continued their usual lifestyle. The limited availability of arable farmlands in karst valleys, basins, or closed depressions drives farmers to reclaim land on sloping ground. Disturbances (fire, fuel wood harvesting, and grazing) also occurred on this ecologically fragile karst area

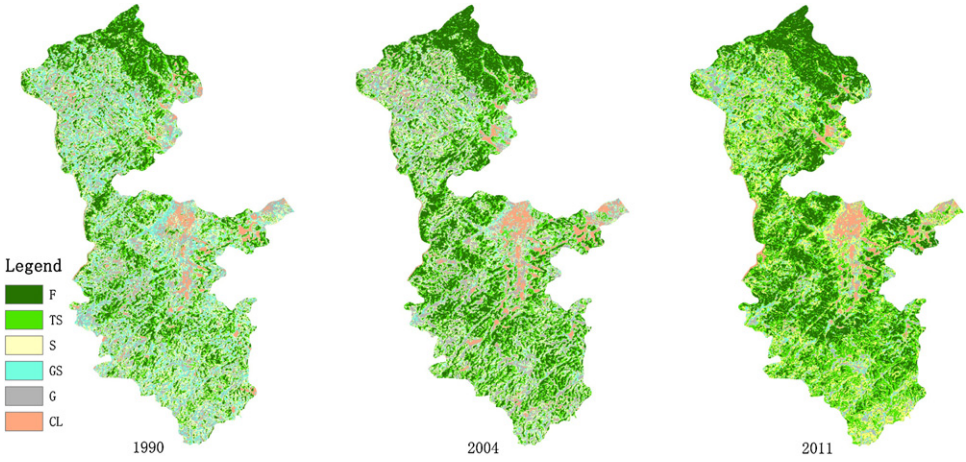

Fig. 4. Spatial distribution of vegetation successional stages in 1990 (a), 2004 (b), and 2011 (c). Note: F, forest; TS, tree–shrub; S, shrub; GS, grass–shrub; G, grass; CL, cropland.

during the study period (Yang et al., 2011). As a result, some vegetation communities degraded, especially those close to villages with high intensity and frequency of anthropogenic disturbances. In addition, interviews with local residents indicated that the grain and financial subsidies from the Green for Grain program were not provided to all farmers, especially those that lived in remote karst areas. Thus, these farmers were not motivated to abandon sloping cropland to allow vegetation recovery.

Although the decrease of percentage of agricultural income in GDP appeared to positively affect vegetation recovery (Table 4), the agricultural income still accounted for a large proportion of GDP. High agriculture production suggests strong pressure on the land. In karst regions, minimizing potential disturbances to soil and reducing soil erosion are critical for sustainable agricultural development, slope stability, and vegetation restoration (Wang et al., 2004b). Changes in agricultural practices are one of the most effective methods for reducing soil disturbance. Over the study period, crops shifted from natural vegetation or corn to forage grass, which reduced effects from grazing on vegetation communities. Meanwhile, forage grass not only proved better for soil conservation, but also for animal husbandry, leading to higher economic growth compared to that from corn or soybean production (Chen et al., 2012). Consequent increases in income can reduce destructive effects of farming on the natural environment.

4. Conclusions

Ecological restoration projects instituted in the 1990s and continuing today have contributed to the recovery of vegetation communities in a degraded karst region in southwest China. This study utilized Landsat imagery from 1990, 2004, and 2011 to examine changes in vegetation communities. Prior to image classification, it is necessary to reduce topographic effects in satellite imagery. The effect of rugged karst terrain in Landsat imagery was reduced by a combination of the inverse of MNF bands, NDMI, and MSI. As a result, the accuracy of the vegetation successional stage classification increased by approximately 20%. The image preprocessing method used in this study could be applied to assess ecological projects in other mountainous regions.

The karst environment in southwest China has been improving since the 1990s. Vegetation communities of early successional stages have evolved to later successional stages. From 1990 to 2011, the percentages of forest and tree–shrub increased by 66.7% and 51.4%, respectively. In contrast, the spatial extent of early successional communities, i.e., shrub, grass–shrub, and grass, decreased by 17.4%, 48.9%, and 53.5%, respectively. Landscape statistics also indicated improvements in vegetation community conditions. Karst vegetation communities became less fragmented, potentially indicating improved conditions of vegetation communities overall. The implementation of the Green for Grain program, mountain closures, and migration program also reduced the dependence of farmers on logging, grazing, and farming on sloping land and contributed to vegetation recovery. However, 14.7% of the vegetation communities in the study area remained degraded, implying that the ecological restoration projects should be continued in karst regions.

Acknowledgments

This study was supported by the Chinese Academy of Sciences Action Plan for the Development of Western China (KZCX2-XB3-10), the National Natural Science Foundation of China (41071340), the National Key Technology Research and Development Program of the Ministry of Science and Technology of China (2010BAE00739-02), and the Western Light Program of Talent Cultivation of the Chinese Academy of Sciences (O923085080). We thank Fu Wei, Zhang Mingyang and Yue Yuemin for providing help in field survey. Lastly, we want to thank the anonymous reviewers who helped to improve the quality of this paper.

References

Chen, H.S., Zhang, W., Wang, K.L., Hou, Y., 2012. Soil organic carbon and total nitrogen as affected by land use types in karst and non-karst areas of northwest Guangxi, China. J. Sci. Food Agric. 92 (5), 1086–1093.
Collins, J.B., Woodcock, C.E., 1996. An assessment of several linear change detection techniques for mapping forest mortality using multitemporal Landsat TM data. Remote Sens. Environ. 56, 66–77.
Crist, E.P., Cicone, R.C., 1984. Application of the tasseled cap concept to simulated thematic mapper data. Photogramm. Eng. Remote Sens. 50, 343–352.
Cuo, L., Vogler, J.B., Fox, J.M., 2010. Topographic normalization for improving vegetation classification in a mountainous watershed in Northern Thailand. Int. J. Remote Sens. 31, 3037–3050.
Dong, L.X., Wang, W.K., Ma, M.G., Kong, J.L., Veroustraete, F., 2009. The change of land cover and land use and its impact factors in upriver key regions of the Yellow River. Int. J. Remote Sens. 30, 1251–1265.
Elvidge, C., Lyon, R., 1985. Influence of rock–soil spectral variation on the assessment of green biomass. Remote Sens. Environ. 17, 265–279.
Foody, G.M., Palubinskas, G., Lucas, R.M., Curran, P.J., Honzak, M., 1996. Identifying terrestrial carbon sinks: classification of successional stages in regenerating tropical forest from Landsat TM data. Remote Sens. Environ. 55, 205–216.
Franklin, S.E., Moskal, L.M., Lavigne, M.B., Pugh, K., 2000. Interpretation and classification of partially harvested forest stands in the Fundy model forest using multitemporal Landsat TM digital data. Can. J. Remote Sens. 26 (4), 318–333.
Franklin, S.E., Lavigne, M.B., Wulder, M.A., McCaffrey, T.M., 2002. Large-area forest structure change detection: an example. Can. J. Remote Sens. 28, 588–592.
Gao, Y.N., Zhang, W.C., 2009. A simple empirical topographic correction method for ETM plus imagery. Int. J. Remote Sens. 30 (9), 2259–2275.
Genet, M., Stokes, A., Fourcaud, T., Norris, J.E., 2010. The influence of plant diversity on slope stability in a moist evergreen deciduous forest. Ecol. Eng. 36, 265–275.
Goodale, C.L., Apps, M.J., Birdsey, R.A., Field, C.B., Heath, L.S., Houghton, R.A., et al., 2002. Forest carbon sinks in the Northern Hemisphere. Ecol. Appl. 21, 891–899.
Green Committee Offices of Guangxi Region, 2001. Guangxi Autonomous Region started pilot governance project of rocky desertification. Land Green. 4, 37.
Green, A.A., Berman, M., Switzer, P., Craig, M.D., 1988. A transformation for ordering multispectral data in terms of image quality with implications for noise removal. IEEE Trans. Geosci. Remote Sens. 26, 65–74.
He, X.Y., Wang, K.L., Zhang, W., Chen, Z.H., Zhu, Y.G., Chen, H.S., 2008. Positive correlation between soil bacterial metabolic and plant species diversity and bacterial and fungal diversity in a vegetation succession on Karst. Plant Soil 307, 123–134.
Helmer, E.H., Brown, S., Cohen, W.B., 2000. Mapping montane tropical forest successional stage and land use with multi-date Landsat imagery. Int. J. Remote Sens. 21, 2163–2183.
Huang, Q.H., Cai, Y.L., 2009. Mapping karst rock in Southwest China. Mt. Res. Dev. 29, 14–20.
Jin, S., Sader, S.A., 2005. Comparison of time series tasseled cap wetness and the normalized difference moisture index in detecting forest disturbances. Remote Sens. Environ. 94, 364–372.
Kuplich, T.M., 2006. Classifying regenerating forest stages in Amazonia using remotely sensed images and a neural network. For. Ecol. Manage. 234, 1–9.
Lee, T.M., Yeh, H.C., 2009. Applying remote sensing techniques to monitor shifting wetland vegetation: a case study of Danshui River estuary mangrove communities, Taiwan. Ecol. Eng. 35, 487–496.
Legrand, H.E., 1973. Hydrological and ecological problems of karst regions. Science 179, 859–864.
Li, E.X., Jiang, Z.C., Cao, J.H., Jiang, G.H., Deng, Y., 2004. The comparison of properties of Karst soil and Karst erosion ratio under different successional stages of Karst vegetation in Nongla, Guangxi. Acta Ecol. Sin. 24, 1131–1139.
Liu, Q.J., Takamura, T., Takeuchi, N., Shao, G., 2002. Mapping of boreal vegetation of a temperate mountain in China by multitemporal LANDSAT imagery. Int. J. Remote Sens. 23, 3385–3405.
Liu, W., Song, C., Schroeder, T.A., Cohen, W.B., 2008. Predicting forest successional stages using multitemporal Landsat imagery with forest inventory and analysis data. Int. J. Remote Sens. 29, 3855–3872.
Lucas, R.M., Honzak, M., Amaral, I.D., Curran, P.J., Foody, G.M., 2002. Forest regeneration on abandoned clearances in central Amazonia. Int. J. Remote Sens. 23 (5), 965–988.
Lyon, J.G., Yuan, D., Lunetta, R.S., Elvidge, C.D., 1998. A change detection experiment using vegetation indices. Photogramm. Eng. Remote Sens. 64, 143–150.
Mello, A.Y.I., Alves, D.S., 2011. Secondary vegetation dynamics in the Brazilian Amazon based on thematic mapper imagery. Remote Sens. Lett. 2, 189–194.
Nie, Y.P., Chen, H.S., Wang, K.L., Yang, J., 2012. Water source utilization by woody plants growing on dolomite outcrops and nearby soils during dry seasons in karst region of Southwest China. J. Hydrol. 420, 264–274.
Parise, M., Gunn, J., 2007. Natural and anthropogenic hazards in karst areas: recognition, analysis and mitigation. J. Geol. Soc. Lond. 279, 1–3.

Peng, W.X., Song, T.Q., Zeng, F.P., Wang, K.L., Du, H., Lu, S.Y., 2012. Relationships between woody plants and environmental factors in karst mixed evergreen-deciduous broadleaf forest, southwest China. J. Food Agric. Environ. 10, 890–896.

Pregitzer, K.S., Euskirchen, E.S., 2004. Carbon cycling and storage in world forests: biome patterns related to forest age. Glob. Change Biol. 10 (12), 2052–2077.

Riano, D., Chuvieco, E., Salas, J., Aguado, I., 2003. Assessment of different topographic corrections in Landsat-TM data for mapping vegetation types. IEEE Trans. Geosci. Remote Sens. 41, 1056–1061.

Roy, P.S., Sharma, K.P., Jain, A., 1996. Stratification of density in dry deciduous forest using satellite remote sensing digital data – an approach based on spectral indices. J. Biosci. 21, 723–734.

Schroeder, T.A., Cohen, W.B., Yang, Z., 2007. Patterns of forest regrowth following clearcutting in western Oregon as determined from a Landsat time-series. For. Ecol. Manage. 243, 259–273.

Senoo, T., Kobayashi, F., Tanaka, S., Sugimura, T., 1990. Improvement of forest type classification by SPOT HRV with 20 m mesh DTM. Int. J. Remote Sens. 11, 1011–1022.

Smith, J.A., Tzeu, L.L., Ranson, K.J., 1980. The Lambertian assumption and Landsat data. Photogramm. Eng. Remote Sens. 46 (10), 1183–1189.

Song, C.H., Schroeder, T.A., Cohen, W.B., 2007. Predicting temperate conifer forest successional stage distributions with multitemporal Landsat Thematic Mapper imagery. Remote Sens. Environ. 106, 228–237.

Song, C.H., Woodcock, C.E., 2002. The spatial manifestation of forest succession in optical imagery: the potential of multiresolution imagery. Remote Sens. Environ. 82, 271–284.

Song, C.H., Woodcock, C.E., Seto, K.C., Pax-Lenney, M., Macomber, S.A., 2001. Classification and change detection using Landsat TM data: when and how to correct atmospheric effects. Remote Sens. Environ. 75, 230–244.

Song, C.H., Woodcock, C.E., 2003. Monitoring forest succession with multitemporal Landsat images: factors of uncertainty. IEEE Trans. Geosci. Remote Sens. 41, 2557–2567.

Stokes, A., Sotir, R., Chen, W., Ghestem, M., 2010. Soil bio- and eco-engineering in China: past experience and future priorities. Ecol. Econ. 36, 247–257.

Su, W.C., 2002. Controlling model for rocky desertification of karst mountainous region and its preventing strategy in Southwest China. J. Soil. Water Conserv. 16, 29–32 (in Chinese).

Tang, C.Q., Zhao, M.H., Li, X.S., Ohsawa, M., Ou, X.K., 2010. Secondary succession of plant communities in a subtropical mountainous region of SW China. Ecol. Res. 25, 149–161.

Teillet, P.M., Guindon, B., Goodenough, D.G., 1982. On the slope-aspect correction of multispectral scanner data. Can. J. Remote Sens. 8, 1537–1540.

Tokola, T., Sarkeala, J., Linden, M.V.D., 2001. Use of topographic correction in Landsat TM-based forest interpretation in Nepal. Int. J. Remote Sens. 22 (4), 551–563.

Verbesselt, J., Hyndman, R., Newnham, G., Culvenor, D., 2010. Detecting trend and seasonal changes in satellite image time series. Remote Sens. Environ. 114, 106–115.

Wang, S.J., Li, R.L., Sun, C.X., Zhang, D.F., Li, F.Q., Zhou, D.Q., Xiong, K.N., Zhou, Z.F., 2004a. How types of carbonate rock assemblages constrain the distribution of karst rocky desertified land in Guizhou Province. PR China: phenomena and mechanisms. Land Degrad. Dev. 15, 123–131.

Wang, S.J., Liu, Q.M., Zhang, D.F., 2004b. Karst rocky desertification in southwestern China: geomorphology, landuse, impact and rehabilitation. Land Degrad. Dev. 15, 115–121.

Wen, Y.G., Sun, D.J., Zhu, H.G., Liu, J.T., Liu, S.R., Shi, Z.M., 2011. Changes in aboveground biomass and diversity between different stages of secondary succession of a karst vegetation in Guangxi, China. In: Hu, J. (Ed.), Advances in Biomedical Engineering. Information Engineering Research Inst, Newark, USA.

Wilson, E.H., Sader, S.A., 2002. Detection of forest harvest type using multiple dates of Landsat TM imagery. Remote Sens. Environ. 80, 385–396.

Woo, M.K., Fang, G.X., DiCenzo, P.D., 1997. The role of vegetation in the retardation of soil erosion. Catema 29 (2), 145–159.

Yang, Q.Q., Wang, K.L., Zhang, C.H., Yue, Y.M., Tian, R.C., Fan, F.D., 2011. Spatio-temporal evolution of rocky desertification and its driving forces in karst areas of Northwestern Guangxi, China. Environ. Earth Sci. 64, 383–393.

Yu, L.F., Zhu, S.Q., Ye, J.Z., Wei, L.M., Chen, Z.G., 2000. A study on evaluation of natural restoration for degraded karst forest. Sci. Silvae Sinicae 36 (6), 12–19 (in Chinese).

Yu, D.Y., Shi, P.J., Han, G.Y., Zhu, W.Q., Du, S.Q., Xun, B., 2011. Forest ecosystem restoration due to a national conservation plan in China. Ecol. Eng. 37, 1387–1397.

Zhang, M.Y., Wang, K.L., Zhang, C.H., Chen, H.S., Liu, H.Y., Yue, Y.M., Ingrid, L., Qi, X.K., 2011. Using the radial basis function network model to assess rocky desertification in northwest Guangxi, China. Environ. Earth Sci. 62, 69–76.